



A98-16092

AIAA 98-0171

**Analysis of Hypersonic Viscous Flow About Bluff
Cylinders Placed One After Another**

I. V. Yegorov and M. V. Yegorova

Central Aero-Hydrodynamics Institute (TsAGI)

Zhukovsky-3, Moscow region, Russia

and

V. V. Riabov

Daniel Webster College

Nashua, New Hampshire, USA

**36th Aerospace Sciences
Meeting & Exhibit**

January 12–15, 1998 / Reno, NV

ANALYSIS OF HYPERSONIC VISCOUS FLOW ABOUT BLUFF CYLINDERS PLACED ONE AFTER ANOTHER

I. V. Yegorov* and M. V. Yegorova†

*Central Aero-Hydrodynamics Institute
Zhukovsky-3, Moscow region, Russia 140160*

and

V. V. Riabov‡

*Daniel Webster College
Nashua, New Hampshire 03063-1300, USA*

Abstract

The flow structure about two bluff cylinders placed one after another in hypersonic viscous flow has been studied. The grid equations approximated the Navier-Stokes equations were solved numerically by application of the implicit monotonized scheme of second-order accuracy, the modified Newton's method, and the Christoffel-Schwarz grid-transformation technique. The similarity conditions of developing fully subsonic zone with recirculating between the cylinders have been discussed. The changes of temperature, pressure and velocity fields in the wakes behind the cylinders, as well as skin friction and heat flux along cylinder surfaces have been analyzed.

Nomenclature

C_f = local skin friction coefficient
 C_x = drag coefficient
 c_p, c_v = specific heats at constant pressure and volume
 e = total energy per unit volume, $\rho(c_p T + (u^2 + v^2)/2)$
 \mathbf{E}, \mathbf{G} = flux-vectors in curvilinear coordinate system
 H = total enthalpy per unit volume, $c_p T + (u^2 + v^2)/2$
 h = node size
 J = Jacobian of the coordinates transformation
 k = Boltzmann's constant
 m = molecular mass
 Pr = Prandtl number
 p = pressure, $\rho k T / m$

\mathbf{Q} = vector of dependent variables, Eq. (1)

\mathbf{q} = heat flux vector

Re = Reynolds number, $\rho u r / \mu$

r = radius of the cylinder

T = temperature

u, v = x - and y - velocity components

x, y = Cartesian coordinates

γ = specific heat ratio, c_p / c_v

Δ = distance between the cylinders

η = curvilinear coordinate

λ_i = eigenvalue

μ = viscosity coefficient

ξ = curvilinear coordinate

ρ = density of fluid

τ = viscous stress tensor

τ_k = regularization parameter, Eq. (11)

Subscripts

c = Cartesian coordinate system

w = wall value

∞ = freestream value

Introduction

The structure of incompressible viscous flow between the cylinders in tandem was studied in detail by many researches (i.e., see a review of Blevins¹). It was found that drag on downstream cylinder was very sensitive to the distance between the centers of cylinders, Δ , and it even changed sign at $\Delta/r < 2$. The case of compressible viscous flow between the cylinders has not been discussed yet. The Reynolds number can play a fundamental role in studying aerothermodynamic characteristics of the bluff bodies. In

*Leading Scientist, Aerothermodynamics Division.

†Research Scientist, Aerothermodynamics Division.

‡Adjunct Associate Professor, Department of Engineering, Mathematics and Science, 20 University Drive. Member AIAA.

Copyright © 1997 by the American Institute of Aeronautics and Astronautics, Inc. All rights reserved.

our previous paper², we analyzed the two-dimensional hypersonic viscous flow about a plate placed in the wake of the cylinder. The strong influence of the Reynolds number and of the geometrical interference factor on skin friction and heat flux along the body surfaces have been found.

In the present analysis, the structure of hypersonic viscous flow about two bluff cylinders in tandem has been studied. This flow pattern would be an appropriate model of measurement devices, tools for controlling separation and recirculation zones, fuel-combustion techniques, and, after certain modification, it can be used to simulate hypersonic viscous flow about projectiles. The analysis of two-dimensional flow structure is based on numerical solutions of the Navier-Stokes equations using an implicit monotonized scheme of second-order accuracy (Total Variation Diminishing scheme) and Newton's method for solving the grid equations.² The influence of the Reynolds number and the geometrical factor, Δ/r , on skin-friction, heat flux, pressure and temperature distributions in the flow and along the surfaces of the cylinders has been studied.

Navier-Stokes Equations and Boundary Conditions.

The unsteady two-dimensional Navier-Stokes equations in a curvilinear coordinate system (ξ, η) , $x = x(\xi, \eta)$, $y = y(\xi, \eta)$, where x, y are Cartesian coordinates have a conservation form:^{3,4}

$$\frac{\partial \mathbf{Q}}{\partial t} + \frac{\partial \mathbf{E}}{\partial \xi} + \frac{\partial \mathbf{G}}{\partial \eta} = 0 \quad (1)$$

Here \mathbf{Q} is a dependent-variables vector, \mathbf{E} and \mathbf{G} are flux-vectors in curvilinear coordinate system. \mathbf{Q} , \mathbf{E} and \mathbf{G} vectors are corresponding to Cartesian vectors \mathbf{Q}_c , \mathbf{E}_c , and \mathbf{G}_c as follow:

$$\begin{aligned} \mathbf{Q} &= J \mathbf{Q}_c; \quad \mathbf{E} = J \left(\mathbf{E}_c \frac{\partial \xi}{\partial x} + \mathbf{G}_c \frac{\partial \xi}{\partial y} \right) \\ \mathbf{G} &= J \left(\mathbf{E}_c \frac{\partial \eta}{\partial x} + \mathbf{G}_c \frac{\partial \eta}{\partial y} \right) \end{aligned} \quad (2)$$

where $J = \partial(x, y) / \partial(\xi, \eta)$ is a Jacobian of the coordinates' transformation.

The Cartesian vector components \mathbf{Q}_c , \mathbf{E}_c , and \mathbf{G}_c for the two-dimensional Navier-Stokes equations have the following form:

$$\begin{aligned} \mathbf{Q}_c &= \begin{pmatrix} \rho \\ \rho u \\ \rho v \\ e \end{pmatrix} \\ \mathbf{E}_c &= \begin{pmatrix} \rho u \\ \rho u^2 + p - \tau_{xx} \\ \rho uv - \tau_{xy} \\ \rho u H - q_x \end{pmatrix} \\ \mathbf{G}_c &= \begin{pmatrix} \rho v \\ \rho uv - \tau_{xy} \\ \rho v^2 + p - \tau_{yy} \\ \rho v H - q_y \end{pmatrix} \end{aligned} \quad (3)$$

The viscous stress tensor τ and the heat flux vector \mathbf{q} have been calculated by formulas given in Ref. 2. Also, it is assumed that the viscosity is approximated by the law, $\mu/\mu_\infty = (T/T_\infty)^{0.7}$, and the Prandtl number is constant, $Pr = 0.7$.

For further numerical analysis, new non-dimensional parameters in Eqs. (1) - (3) were set up by normalizing the Cartesian coordinates to the characteristic length scale r (the radius of a cylinder), the Cartesian velocity components - to the upstream velocity u_∞ , the pressure - to the double value of the dynamic pressure in upstream flow, and other parameters - to their values in upstream flow.

To complete the finite-differences system of the Navier-Stokes equations, following boundary conditions have been used. The no-slip conditions ($u = v = 0$), constant wall temperature ($T = T_w$), and extrapolations of pressure from inner area nodes (with the condition $\partial p / \partial \eta = 0$) were posed on the body surface. On the outer surface of the computational area around the body, boundary conditions were written in the form of Riemann invariants and determined by the direction of perturbation expansion⁴.

The Approximation of Equations

The construction of a finite-difference scheme to solve the Navier-Stokes equations (1) given in conservation laws form is based upon an integro-interpolation method.⁴ The utilization of an integro-interpolation method applied to the

solution of the Navier-Stokes equations gives finite-differences conservation law analogies:

$$\frac{\mathbf{Q}_{j,k}^{n+1} - \mathbf{Q}_{j,k}^n}{\tau} + \frac{\mathbf{E}_{j+\frac{1}{2},k}^{n+1} - \mathbf{E}_{j-\frac{1}{2},k}^{n+1}}{h_\xi} + \frac{\mathbf{G}_{j,k+\frac{1}{2}}^{n+1} - \mathbf{G}_{j,k-\frac{1}{2}}^{n+1}}{h_\eta} = \mathbf{B}_{j,k}^{n+1} \quad (4)$$

Here index n corresponds to time layer number; j, k - to node numbers along ξ and η , correspondingly; h_ξ, h_η - to the node sizes. The developed conservative finite-difference scheme is implicit, and this property of the scheme allows to avoid any restrictions on the iteration time-step caused by the instability of the ordinary difference schemes in the solution of the stiff differential equations.

At semi-integer nodes, the convective components of the flux vectors \mathbf{E} and \mathbf{G} were approximated using a monotonized scheme of the Godunov's type.⁵ The eigenvalues and eigenvectors at semi-integer nodes were calculated by the Roe's method⁶, for the approximate solution of the problem of arbitrary discontinuity decay:

$$\mathbf{E}_{j+\frac{1}{2}} = \frac{1}{2}(\mathbf{E}(\mathbf{Q}_L) + \mathbf{E}(\mathbf{Q}_R)) - \mathbf{R}(\mathbf{Q}_{LR}) \Phi(\Lambda_{LR}) \mathbf{R}(\mathbf{Q}_{LR})^{-1} (\mathbf{Q}_R - \mathbf{Q}_L) \quad (5)$$

Here $\Phi(\Lambda_{LR})$ is a diagonal matrix with elements $\phi(\lambda_j)$; parameters λ_j are the eigenvalues of the operator $\mathbf{A} = \partial \mathbf{E} / \partial \mathbf{Q}$; and $\mathbf{R}_{LR} = \mathbf{R}(\mathbf{Q}_{LR})$ is a matrix with the columns being the right-hand side eigenvectors of the operator \mathbf{A} . The function $\phi(\lambda)$ has the form, which satisfies the "entropy" condition (or the criterion) in the choosing of a numerical solution with the correct physical properties.²

To increase the order of finite-difference approximations up to the second one, the Monotone-Upstream-Scheme-for-Conservation-Laws principle of the minimum derivatives⁷ was used to interpolate dependent variables on the node side as follows:

$$\begin{aligned} \mathbf{Q}_L &= \mathbf{Q}_j + \frac{1}{2} \min \text{mod}(\mathbf{Q}_j - \mathbf{Q}_{j-1}, \mathbf{Q}_{j+1} - \mathbf{Q}_j), \\ \mathbf{Q}_R &= \mathbf{Q}_j - \frac{1}{2} \min \text{mod}(\mathbf{Q}_{j+1} - \mathbf{Q}_j, \mathbf{Q}_{j+2} - \mathbf{Q}_{j+1}) \end{aligned} \quad (6)$$

The function $\min \text{mod}(a, b)$ has the form:

$$\min \text{mod}(a, b) = \begin{cases} a, & ab > 0, \quad |a| < |b| \\ b, & ab > 0, \quad |a| \geq |b| \\ 0, & ab \leq 0 \end{cases} \quad (7)$$

The Roe's method⁶ to solve approximately the Riemann's problem of arbitrary discontinuity decay was utilized to compute eigenvalues and eigenvectors of the \mathbf{A} -operator. Parameters $\Phi(\Lambda_{LR}), \mathbf{R}_{LR}, \mathbf{R}_{LR}^{-1}$ were calculated by the values of dependent variables, such as:

$$\begin{aligned} u_{LR} &= \frac{u_L \sqrt{\rho_L} + u_R \sqrt{\rho_R}}{\sqrt{\rho_L} + \sqrt{\rho_R}} \\ v_{LR} &= \frac{v_L \sqrt{\rho_L} + v_R \sqrt{\rho_R}}{\sqrt{\rho_L} + \sqrt{\rho_R}} \\ c_{LR} &= \frac{c_L \sqrt{\rho_L} + c_R \sqrt{\rho_R}}{\sqrt{\rho_L} + \sqrt{\rho_R}} \end{aligned} \quad (8)$$

Here the parameter c indicates the local speed of sound.

The diffusion components of the flux vectors \mathbf{E} and \mathbf{G} at the node side were approximated by the second order central difference scheme:

$$\begin{aligned} \frac{\partial \mathbf{U}}{\partial \xi_{j+\frac{1}{2},k}} &= \frac{\mathbf{U}_{j+1,k} - \mathbf{U}_{j,k}}{h_\xi} \\ \frac{\partial \mathbf{U}}{\partial \eta_{j+\frac{1}{2},k}} &= \frac{\mathbf{U}_{j+1,k+1} + \mathbf{U}_{j,k+1} - \mathbf{U}_{j+1,k-1} - \mathbf{U}_{j,k-1}}{4h_\eta} \end{aligned} \quad (9)$$

Here the parameter \mathbf{U} is a vector of non-conservative dependent variables.

The difference scheme pattern used for the approximation of the complete Navier-Stokes equations consists of 13 nodes. It was found, that the developed implicit nonlinear finite-difference scheme is absolutely stable in the case of the linear problem.

In present study, the numerical algorithm developed for

the internal flow modeling has been adopted to study external hypersonic viscous flows. The construction of the computational mesh was made by numerical solution of the Christoffel-Schwarz transformation problem.^{8,9} The technique of the mesh adaptation in the boundary layers at high Reynolds numbers¹⁰ has been used in this study.

Solution of Nonlinear Differences Equations

The nonlinear system of grid equations ($\mathbf{F}(\mathbf{X}) = 0$, where \mathbf{X} is a vector of unknown discrete functions) was solved using the modified Newton's method:^{2,3,10}

$$\mathbf{X}^{[k+1]} = \mathbf{X}^{[k]} - \tau_{k+1} \mathbf{D}^{-1} \mathbf{F}(\mathbf{X}^{[k]}) \quad (10)$$

Here $\mathbf{D} = \partial \mathbf{F} / \partial \mathbf{X}$ is the Jacobi matrix; k is the iteration number. In computations, the regularization parameter τ_k was calculated by formula¹¹:

$$\tau_{k+1} = \frac{(\Delta \mathbf{X}^{[k]} - \Delta \mathbf{X}^{[k-1]}, \mathbf{X}^{[k]} - \mathbf{X}^{[k-1]})}{(\Delta \mathbf{X}^{[k]} - \Delta \mathbf{X}^{[k-1]})^2} \quad (11)$$

where $\Delta \mathbf{X}^{[k]}$ is a vector of corrections. The iteration process is convergent with the second order of the convergence rate and $\tau_k \rightarrow 1$.

The iteration Jacobi matrix was found by employing the procedure of finite increments of the residual vector of the required grid functions. The approximation of the Navier-Stokes equations determinates the type of the Jacobi \mathbf{D} -operator, namely, the rarefied structure of triangular matrices and the initial 7×7 -dense matrix coincide.

The system of linear algebraic equations obtained in a nonlinearity iteration was solved by expanding the matrix into a product of two triangular matrices \mathbf{L} and \mathbf{U} , where \mathbf{L} is the lower triangular matrix and \mathbf{U} is the upper triangular matrix, and $\partial \mathbf{F} / \partial \mathbf{X} = \mathbf{L} * \mathbf{U}$. This operation was preceded by the analysis of the sparsity structure of matrices \mathbf{L} and \mathbf{U} . In order to reduce the total number of the arithmetic operations and economize on RAM, the variables were numbered using the generalized method of nested dissection^{12,13}. This technique was successfully used many times in computational experiments and proved its effectiveness and reliability.⁴

Numerical Calculations and Tests

The calculations were mainly performed on the 101×151 grid of the H-type. The size of the nodes was automatically reduced near the body surface and in the vicinity of the symmetry plane. The example of the finite-difference grid in physical space is presented in Fig. 1.

The convergence and accuracy of the numerical solutions were tested by calculating hypersonic viscous flow about a cylinder (at Reynolds number $Re_{\infty r} = 10^4$ and Mach number in upstream flow $M_{\infty} = 5$) on the grids of different size. The analysis of the results³ showed that the numerical solution of the problem is convergent. Calculations were carried out at the Work Station RS6000/58H.

To improve the convergence rate of the iteration process, the new technique of formation of the Jacobi matrix was used. The method is based upon the usage of a truncated 3×3 -dense matrix. The computing time of each variant was reduced by the factor of three and was estimated as approximately 3h. 20 min.

Results

Influence of Reynolds Number

The flowfield around two identical bluff cylinders (with the generatrix $y/r = -0.5 \cos(\pi x/2r)$ and located at $-3 \leq x/r \leq -1$ and $1 \leq x/r \leq 3$, correspondingly) was calculated for a Mach number $M_{\infty} = 5$ and for a Reynolds number $Re_{\infty r} = 300, 10^3, 10^4$ and 10^5 . It was assumed that $\gamma = 1.4$, and the surface is isothermal at $T_w/T_{\infty} = 2$. The distance between the cylinders remains constant, $\Delta/r = 2$, in these study cases.

The contours of constant values of local Mach number M and temperature T/T_{∞} are shown in Figs. 2 and 3, correspondingly, for four cases of the Reynolds numbers. The flow structure changes significantly with increasing the major similarity parameter of the Reynolds number. At $Re_{\infty r} \geq 10^4$, the zone between the cylinders becomes totally subsonic. As a result, the hot-gas area near the down-stream cylinder spreads far up-stream, up to the rear zone of the first cylinder. Behind the second cylinder, the wake area becomes narrow and it is filled with hot gas.

The distributions of flow parameters along the plane of symmetry in the wakes behind the cylinders and along their surfaces are shown in Fig. 4. The Reynolds number influences significantly the pressure, velocity, and Mach

number parameters. At $Re_{\infty} \geq 10^4$, the zone between the cylinders is characterized by complex recirculation processes. The pressure distribution along the surface of the down-stream cylinder changes significantly its pattern. The subsonic recirculation zone is developing behind this cylinder with increasing the Reynolds number.

The normalized distributions of skin-friction coefficient and heat flux along the surfaces of cylinders are shown in Figs. 5 and 6 correspondingly. The developing recirculation zone between the cylinders influences considerably these aerothermodynamic parameters on the rear surface of the first body and on the total surface of the down-stream cylinder. It is an interesting fact that the extreme values of the skin-friction coefficient and heat flux do not coincide with each other at any parameter of the Reynolds number. It indicates that the "Reynolds analogy" takes place only under the conditions of laminar non-separated flow near the up-stream surface of the first cylinder.

The calculating results of the drag coefficient and its two main components (based on skin-friction and pressure distribution analysis) are shown in Fig. 7. At small Reynolds numbers, $Re_{\infty} \leq 10^3$, skin-friction component becomes predominant. This parameter of the first cylinder is larger by factor of 4.5 than the corresponding parameter of the down-stream body. At $Re_{\infty} \geq 10^4$, the pressure-distribution component contributes prevalently into the drag coefficient of both cylinders, and the coefficient of the second cylinder changes non-monotonically with increasing the Reynolds number.

Influence of the Geometrical Factor, Δ/r

The flow pattern is significantly sensitive to the major geometrical similarity parameter, Δ/r , where Δ is a distance between a rear point of the first cylinder and a front (stagnation) point of the second body in tandem. The influence of this parameter on the flow structure has been studied for a Mach number $M_{\infty} = 5$ and for a Reynolds number $Re_{\infty} = 10^4$.

The local Mach number and temperature contours are shown in Figs. 8 and 9, correspondingly, for four cases of a distance between bodies ($\Delta/r = 0.5, 1, 2, \text{ and } 3$). At $\Delta/r \leq 1$, the ordinary wake structure behind the first cylinder is destroyed completely by the up-steaming flow from the second body. In all cases, the core of the wake becomes subsonic with recirculating.

The distributions of Mach number and pressure along the plane of symmetry in the wakes behind the bodies and along their surfaces are shown in Fig. 10. The velocity parameter in the recirculation zone between the cylinders reaches its maximum value at $1 \leq \Delta/r \leq 2$ (see Fig. 10a). At $\Delta/r \geq 3$, this parameter changes non-monotonically in the internal acceleration and deceleration zones of the wake. The maximum pressure parameter on the down-stream cylinder increases monotonically by 10% after increasing the distance between the bodies (see Fig. 10b).

The normalized distributions of skin-friction coefficient and heat flux along the cylinders surfaces are shown in Figs. 11 and 12 correspondingly. The skin-friction coefficient of the first cylinder becomes sensitive to the gasdynamic processes in the recirculation zone between the bodies. This coefficient changes non-monotonically in the rear area of the cylinder with increasing a distance between the cylinders. At $\Delta/r \geq 2$, the skin-friction coefficient and heat flux have become unchangeable in this area.

The main changes in distributions of the parameters C_f and q_w occur in the front area of the down-stream body (see Figs. 11b and 12b). The skin-friction coefficient increases monotonically with increasing the distance factor. The parameter of heat flux reaches its maximum value at $\Delta/r = 2$, and after that it decreases with increasing parameter $\Delta/r \geq 3$. This fact indicates, that the Reynolds analogy is not applicable for the flow parameters in the front area of the second cylinder under the considered flow conditions.

The calculating results of the drag coefficient and its two main components (based on skin-friction and pressure distribution analysis) are shown in Fig. 13. At constant Reynolds number, $Re_{\infty} = 10^4$, pressure-distribution component becomes predominant for both cylinders. Only for the first cylinder, it remains approximately constant with increasing a distance between cylinders. The skin-friction fraction of the drag coefficient, C_{xf} , increases monotonically, which is in a good agreement with data of the skin-friction distributions given in Fig. 11. The pattern of drag-coefficient changes is absolutely different from the data in the case of incompressible viscous flow near cylinders in tandem, which was described by Blevins¹. The discussed results indicate complex gasdynamic processes in the compressible viscous flow about the bluff cylinders.

Summary

The hypersonic viscous flow parameters near two bluff cylinders in-tandem have been evaluated numerically for a wide range of the Reynolds numbers. This parameter influences significantly the distributions of pressure, skin friction and heat flux along the cylinders surfaces as well as the flow parameters in the wakes behind the bodies. At $Re_{\infty} \geq 10^4$, the flow zone between the bluff cylinders has totally become subsonic with recirculating. This effect is responsible for significant change of skin-friction and heat-flux characteristics along the body surfaces. The drag coefficient of the down-stream cylinder changes non-monotonously at high Reynolds numbers ($Re_{\infty} \geq 10^4$).

The existence of maximum velocity parameter in the recirculation zone between the bluff cylinders has been found at $Re_{\infty} = 10^4$ and $1 \leq \Delta/r \leq 2$. The maximum pressure parameter and the skin-friction coefficient on the second cylinder surface increase monotonically by 10% with increasing the distance between the bodies from $\Delta/r = 0.5$ to 3. At the same time, heat flux changes non-monotonically, reaching its maximum value at $\Delta/r = 2$. The Reynolds analogy between distributions of skin-friction and heat-flux characteristics does not take place in these cases.

References

¹Blevins, R. D., *Applied Fluid Dynamics Handbook*, Krieger Publishing Company, Malabar, Florida, 1992.

²Yegorov, I. V., Yegorova, M. V., Ivanov, D. V., and Riabov, V. V., "Numerical Study of Hypersonic Viscous Flow About Plates Located Behind a Cylinder," AIAA Paper, No. 97-25-73, June 1997.

³Bashkin, V. A., Egorov, I. V., and Egorova, M. V., "Supersonic Viscous Perfect Gas Flow Past a Circular Cylinder," *Fluid Dynamics*, No. 6, 1993, pp. 833-838.

⁴Yegorov, I., and Zaitsev, O., "Development of Efficient Algorithms for Computational Fluid Dynamic Problems," *Proceedings of the Fifth International Symposium on Computational Fluid Dynamics*, Japan, Sendai, 1993, Vol. III, pp. 393-400.

⁵Godunov, S. K., "Finite Difference Method for Numerical Computation of Discontinuous Solutions of the Equations of Fluid Dynamics," *Matematicheskii Sbornik*, Vol.47, No. 3, 1959, pp. 271-306 (in Russian).

⁶Roe, P. L., "Approximate Riemann Solvers, Parameter Vectors, and Difference Scheme," *Journal of Computational Physics*, Vol. 43, 1981, pp. 357-372.

⁷Kolgan, V. P., "Application of the Principle of Minimum Value of Derivatives to the Construction of Finite-Difference Schemes for Calculating Discontinuous Solutions of Gas Dynamics," *Uchenye Zapiski TsAGI*, Vol. 3, No. 6, 1972, pp. 68-77 (in Russian).

⁸Yegorov, I. V., and Ivanov, D. V., "Application of the Complete Implicit Monotonized Finite-Differential Schemes in Modeling Internal Plane Flows," *Journal of Computational Mathematics and Mathematical Physics*, Vol. 36, No. 12, 1996, pp. 91-107.

⁹Davis, R. T., "Numerical Methods for Coordinate Generation Based on Schwarz-Christoffel Transformations," AIAA Paper, No. 79-1463, June 1979.

¹⁰Bashkin, V. A., Yegorov, I. V., and Ivanov, D. V., "Application of Newton's Method to Calculation of Supersonic Internal Separation Flows," *Journal of Applied Mechanics and Technical Physics*, Vol.38, No.1, 1997, pp. 30-42.

¹¹Karimov, T. Kh., "Some Iteration Methods for Solving Nonlinear Equations in the Hilbert's Space," *Doklady Akademii Nauk SSSR*, Vol. 269, No. 5, 1983, pp. 1038-1042 (in Russian).

¹²Lipton, R. J., Rose, D. J., and Tarjan, R. E., "Generalized Nested Dissection," *SIAM Journal of Numerical Analysis*, Vol. 16, No. 2, 1979, pp. 346-358.

¹³Egorov, I. V., and Zaitsev, O. L., "On an Approach to the Numerical Solution of the Two-Dimensional Navier-Stokes Equations by the Shock Capturing Method," *Journal of Computational Mathematics and Mathematical Physics*, Vol. 31, No. 2, 1991, pp. 286-299.

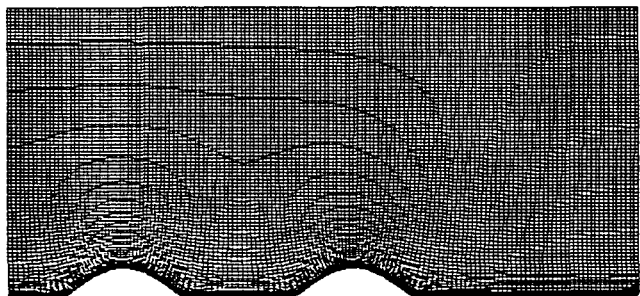
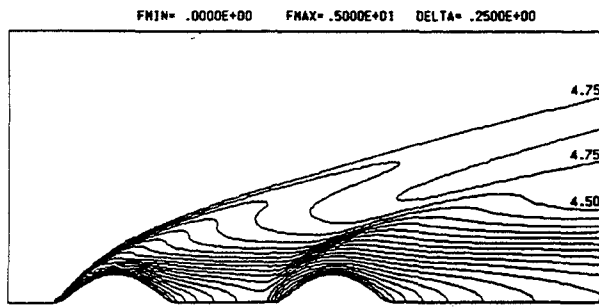
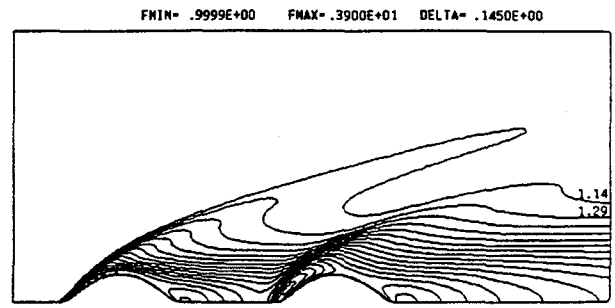


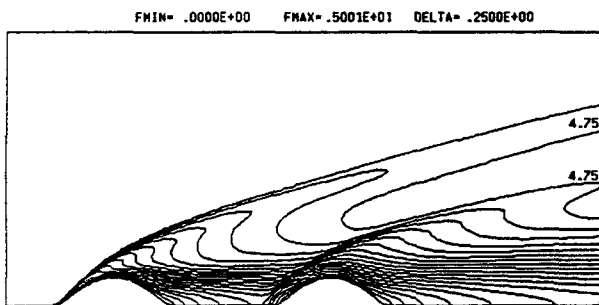
Fig. 1 Finite-difference grid in physical space.



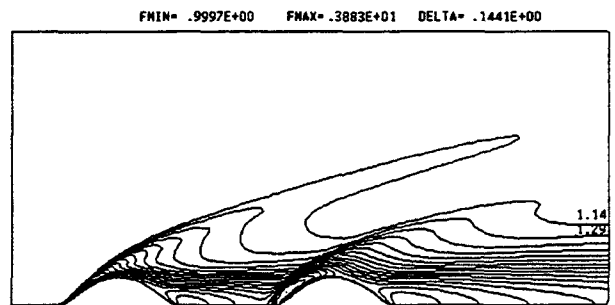
a) $Re = 300$



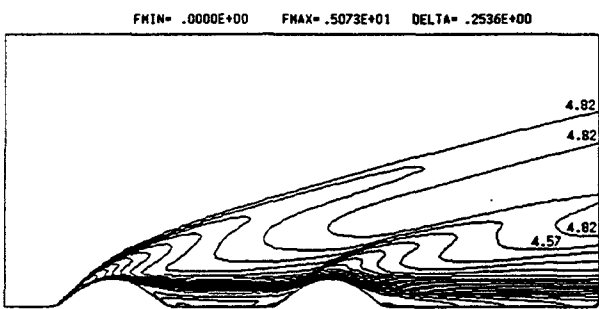
a) $Re = 300$



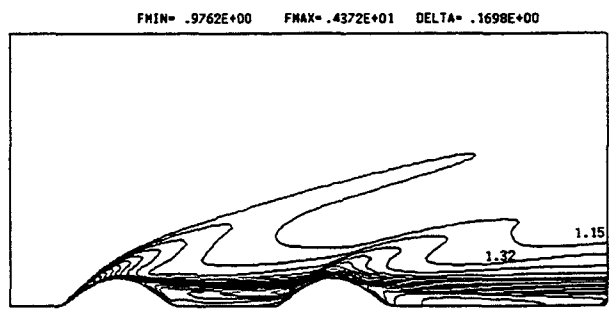
b) $Re = 1000$



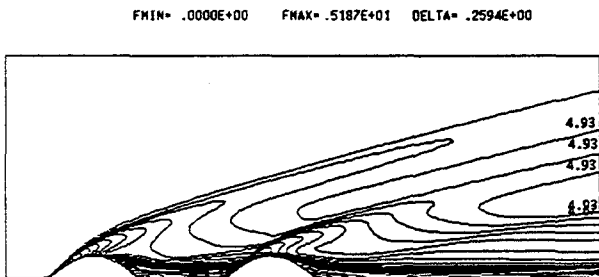
b) $Re = 1000$



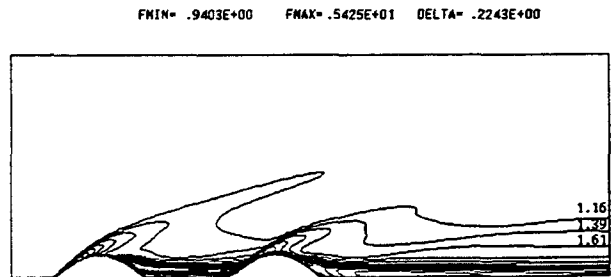
c) $Re = 10^4$



c) $Re = 10^4$



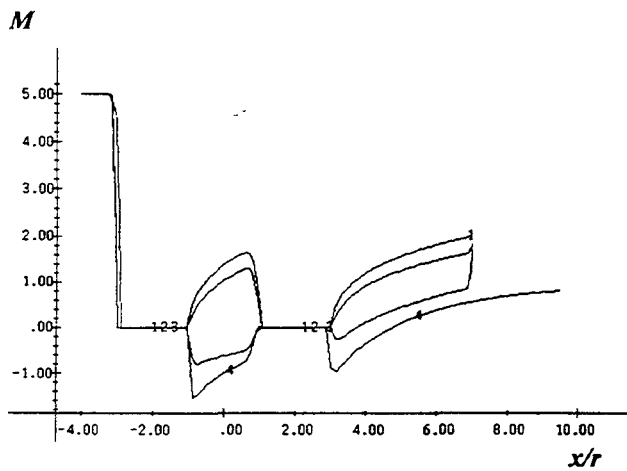
d) $Re = 10^5$



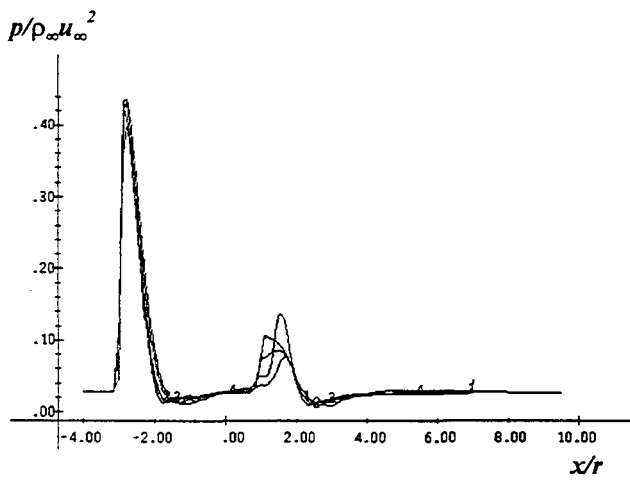
d) $Re = 10^5$

Fig. 2. Mach number contours at $M_\infty = 5$.

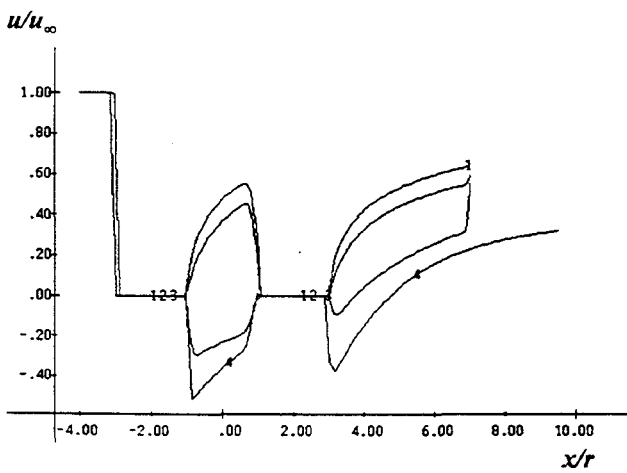
Fig. 3. Temperature contours at $M_\infty = 5$.



a)

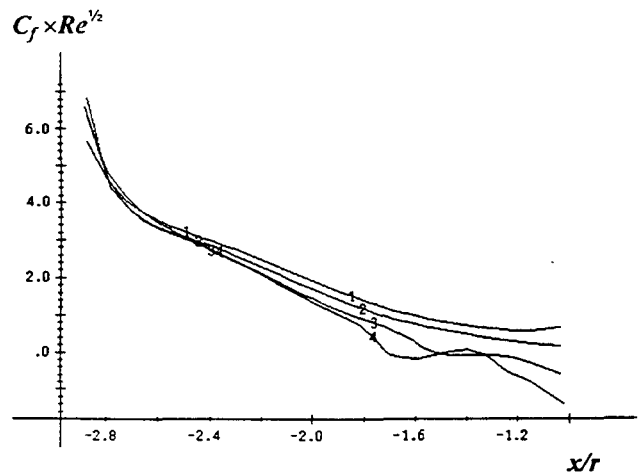


b)

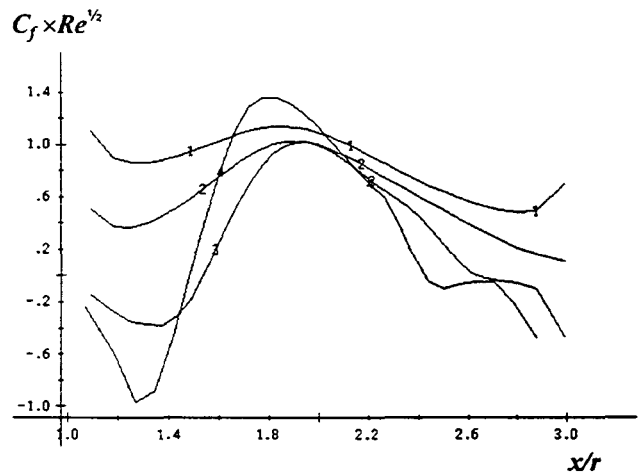


c)

Fig. 4 The flow parameters along the surfaces of cylinders and along the plane of symmetry in the wakes behind the cylinders at $M_\infty = 5$: a) Mach number, M ; b) normalized pressure, $p/\rho_\infty u_\infty^2$; c) normalized velocity, u/u_∞ . Curve 1 - $Re = 300$; curve 2 - $Re = 1000$; curve 3 - $Re = 10^4$; curve 4 - $Re = 10^5$.

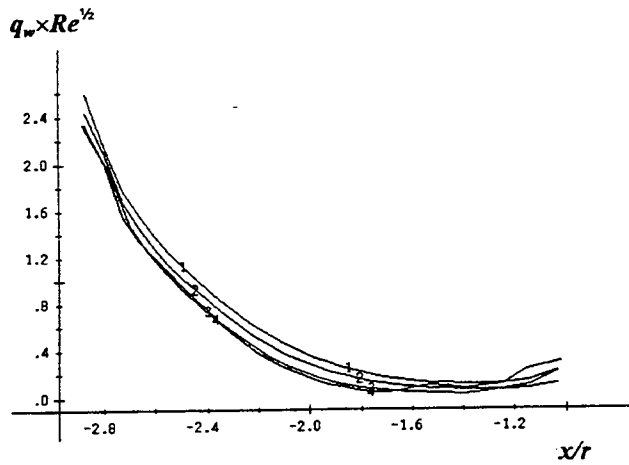


a) first cylinder

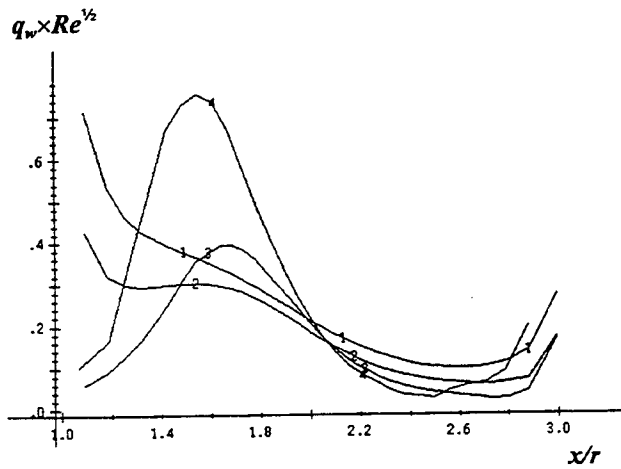


b) second cylinder

Fig. 5 The distribution of skin-friction coefficient, C_f , along the surfaces of cylinders at $M_\infty = 5$: curve 1 - $Re = 300$; curve 2 - $Re = 1000$; curve 3 - $Re = 10^4$; curve 4 - $Re = 10^5$.



a) first cylinder



b) second cylinder

Fig. 6 The distribution of heat flux, q_w , along the surfaces of cylinders at $M_\infty = 5$: curve 1 - $Re = 300$; curve 2 - $Re = 1000$; curve 3 - $Re = 10^4$; curve 4 - $Re = 10^5$.

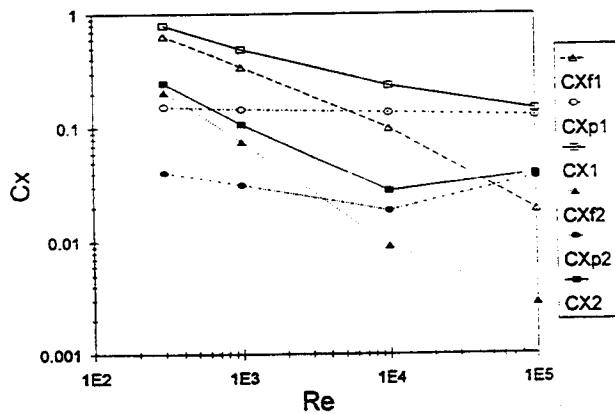
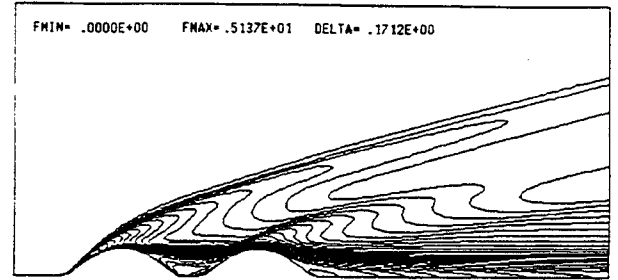
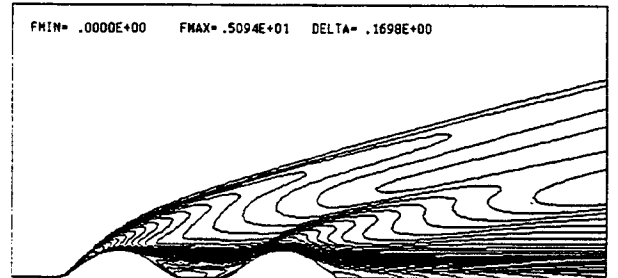


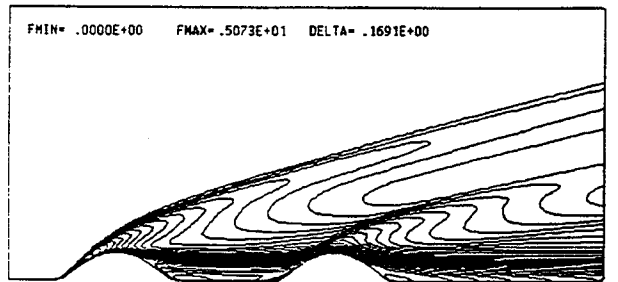
Fig. 7 The drag coefficient C_x vs the Reynolds number $Re_{\infty,r}$ at $M_\infty = 5$: indexes 1 and 2 correspond to the first and second cylinders.



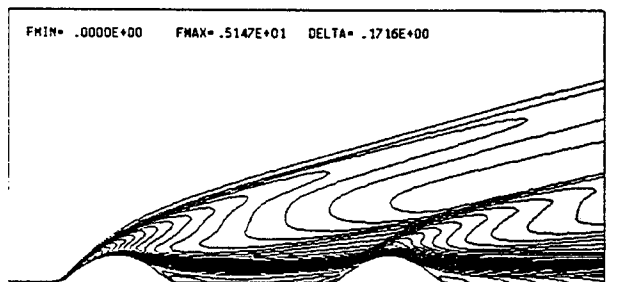
a) $\Delta/r = 0.5$



b) $\Delta/r = 1$

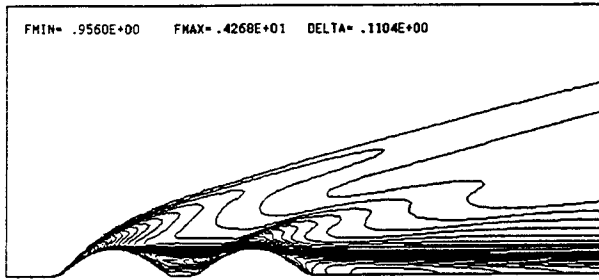


c) $\Delta/r = 2$

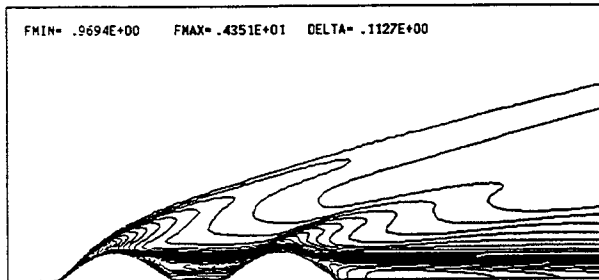


d) $\Delta/r = 3$

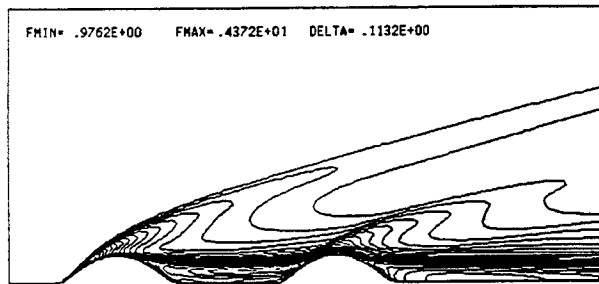
Fig. 8 Mach number contours at $Re = 10^4$



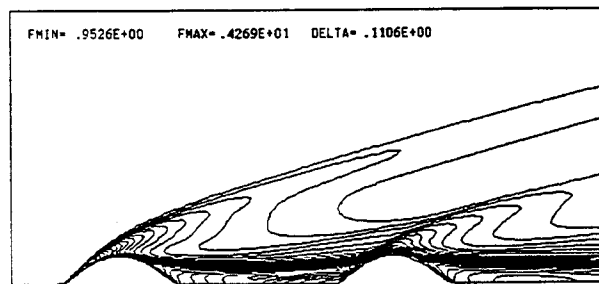
a) $\Delta/r = 0.5$



b) $\Delta/r = 1$

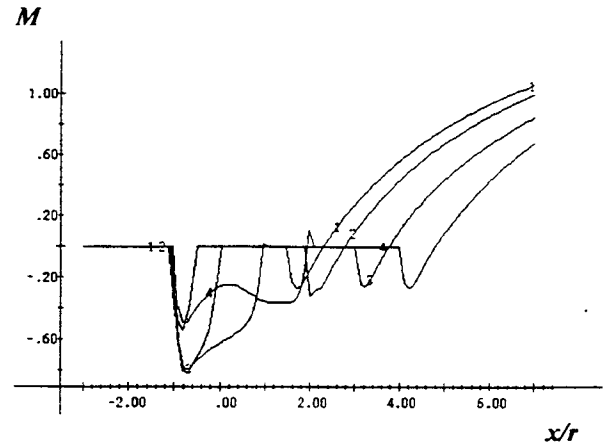


c) $\Delta/r = 2$

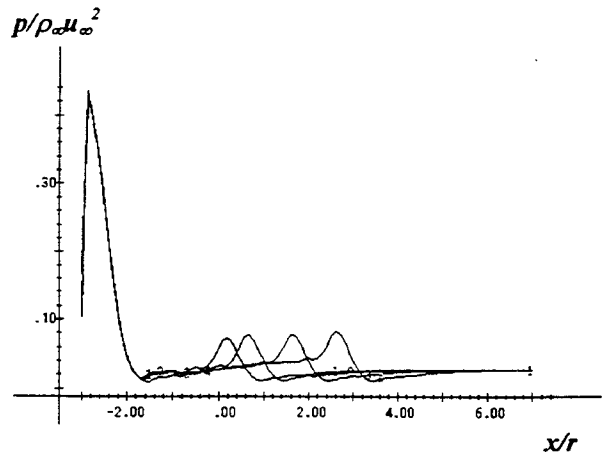


d) $\Delta/r = 3$

Fig. 9 Temperature contours at $Re = 10^4$

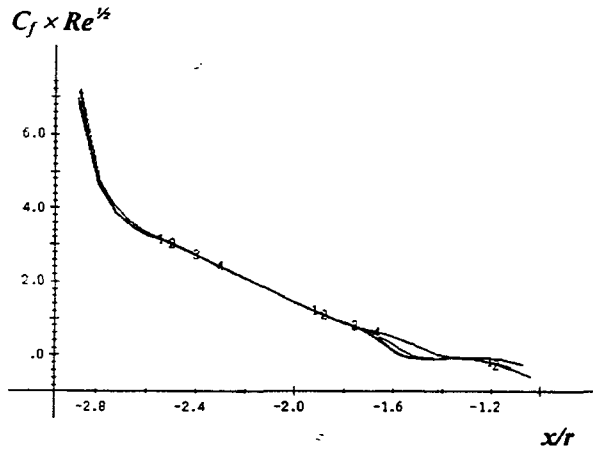


a)

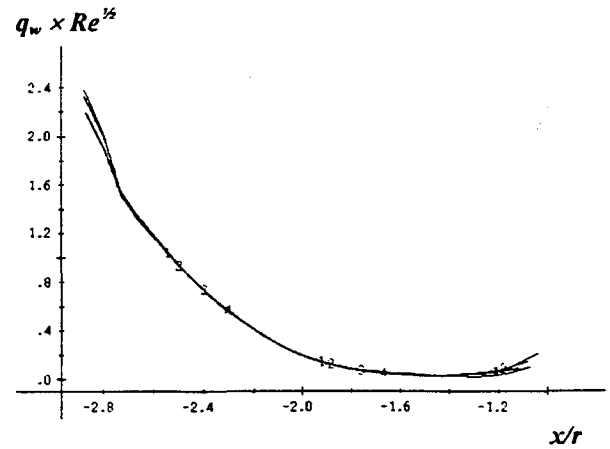


b)

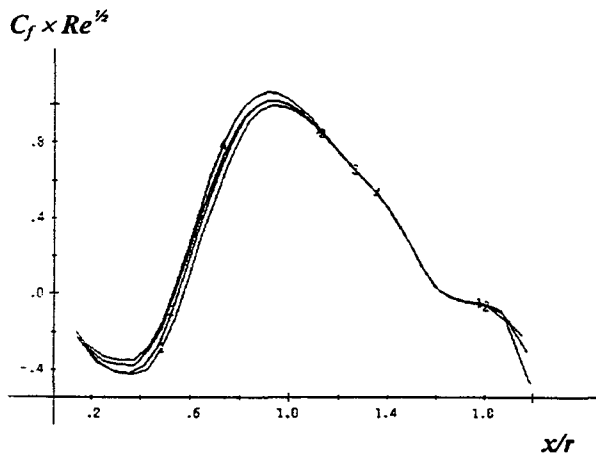
Fig. 10 The flow parameters along the surfaces of cylinders and along the plane of symmetry in the wakes behind the cylinders at $Re = 10^4$: a) Mach number, M ; b) normalized pressure, $p/\rho_\infty U_\infty^2$. Curve 1 - $\Delta/r = 0.5$; curve 2 - $\Delta/r = 1$; curve 3 - $\Delta/r = 2$; curve 4 - $\Delta/r = 3$.



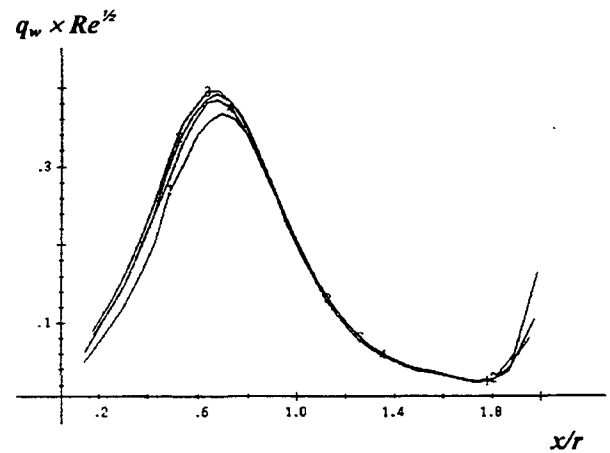
a) first cylinder



a) first cylinder



b) second cylinder



b) second cylinder

Fig. 11 The distribution of skin-friction coefficient, C_f , along the surfaces of cylinders at $Re = 10^4$. Curve 1 - $\Delta r = 0.5$; curve 2 - $\Delta r = 1$; curve 3 - $\Delta r = 2$; curve 4 - $\Delta r = 3$.

Fig. 12 The distribution of heat flux, q_w , along the surfaces of cylinders at $Re = 10^4$. Curve 1 - $\Delta r = 0.5$; curve 2 - $\Delta r = 1$; curve 3 - $\Delta r = 2$; curve 4 - $\Delta r = 3$.

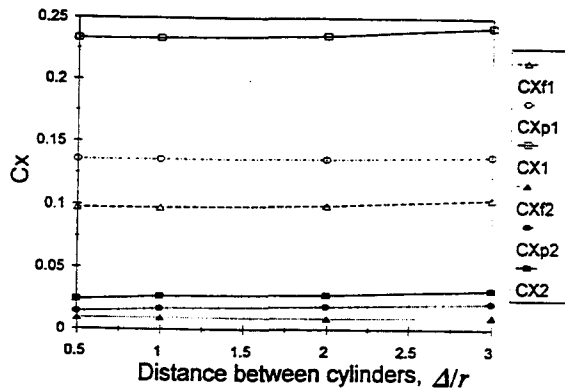


Fig. 13 The drag coefficient C_x vs the distance between the ogival cylinders at Reynolds number $Re_{\infty,r} = 10^4$ and $M_{\infty} = 5$; indexes 1 and 2 correspond to the first and second cylinders.